Iranian Journal of Chemical Engineering, Vol. 20, No. 4, 40-55, (2023)

Iranian Journal of Chemical Engineering

Journal Homepage: www.ijche.com

pISSN: 1735-5397
eISSN: 2008-2355

Special Issue Article

CFD Modeling of the Movement of Bladeless Wind Turbines

A. Das[1], N. Azimi*[1,2]

[1]Department of Chemical Engineering, Faculty of Petroleum and Chemical Engineering, Razi University, Kermanshah, Iran
[2]CFD Research Division, Advanced Chemical Engineering Research Center, Razi University, Kermanshah, Iran

ARTICLE INFO

Article history:
Received: 2024-01-14
Accepted: 2024-02-06
Available online: 2024-02-06

Keywords:
Modeling,
Simulation,
Bladeless wind turbine,
CFD.

ABSTRACT

This research presents the performance of bladeless wind turbines. It also familiarizes readers with the phenomenon of eddy current, which serves as the foundation for bladeless turbines. In this direction, these kinds of bladeless turbines have been designed, modeled, and simulated. Firstly, a two-dimensional vibrational movement of the cylinder with a natural frequency of 2 Hz was modeled at Re = 51000. Additionally, it was noted that the values of the displacement amplitude, and lift coefficient are -0.1-0.1, and -1.5-1.5 respectively. After that, using 2D simulation, the impacts of two different geometries, horizontal and vertical ellipsoids, on displacement amplitude are examined. Investigations were conducted on important factors such as lift coefficients and displacement amplitude, as well as the vortex flow pattern formed behind these shapes. It was discovered that the vertical ellipsoid shape had the maximum values for the height of the displacement amplitude, and lift coefficient. The most important factor influencing the performance of this type of geometry was examined, namely the dimensionless Reynolds number, which ranges from 15000 to 90000. It was determined that the intended geometry exhibited a larger displacement response as the Reynolds number increased.

DOI: 10.22034/ijche.2024.435315.1515 URL: https://www.ijche.com/article_189844.html

1. Introduction

Today, the access to all kinds of new sources of energy, especially clean energy, is very important. Energy is divided into two main categories of renewable and non-renewable according to the source of their production [1-3]. Also, it is no longer possible to rely on existing energy sources and the use of new and clean energies can have a special place [2, 4-6].

*Corresponding author: azimi.neda@razi.ac.ir (N.Azimi)

Among the energies, using wind energy is one of the most comprehensive renewable energy technologies in the world [7-10]. This type of energy is being used to generate electricity via wind turbines. Wind turbines convert the kinetic energy of the wind into mechanical power, which is then transferred to the generator via a shaft and converted into electrical energy. Some models of wind turbines work at constant speed, but variable-speed turbines can produce more energy because their vanes are moved by the forces of lift and drag. Bladeless turbines are one of the newest ideas in the world of small wind turbines [7-8, 11-12]. In the bladeless turbines, electricity is produced by taking advantage of a vibration phenomenon. Bladeless turbines use a sail-shaped body, rotor, and gearbox, unlike conventional bladed turbines. A bladeless wind turbine harvests wind energy through a resonance phenomenon known as vortex shedding that is caused by an aerodynamic effect [2, 13]. When fluid passes through a bluff body, it produces a modified flow and a wake pattern of vortices. Then, the bluff body starts to oscillate and this oscillation is intensified by the fluid. This is called vortex-induced vibration [14-16]. This technology works by placing cylindrical objects in the natural flow of the wind. A bladeless turbine, which captures wind energy from the vortex phenomenon, functions fundamentally as a vortex-induced vibration (VIV) intensification wind generator [13].

Currently, there is a great deal of experimental and numerical research being done on VIV-based energy harvesting. The period of research in the field of oscillating eddy currents, and especially the modeling and simulation of these types of systems, started from the 1990s onward with the expansion and increase of computer systems and their processing power. According to experimental research by Modir et al. [17], the maximum vibration amplitude increases as the mass ratio decreases, as examined by the impact of the mass ratio on the VIV responsiveness of an elastically mounted cylinder. Gohate et al. [18] investigated the performance of an incomplete cone-shaped wind turbine mast. However, their simulation studies were more focused on the scope and possibility of using bladeless turbines, as well as the design of bladeless turbines and the influence of the Reynolds number between 300 and 300,000 and its effect on the behavior of the eddy flow system. Zhang et al. [19] studied the VIV energy harvesting technique. They examined the flow over two bluff objects having various cross sections [19]. They came to the conclusion that the criterion prism performs better in capturing energy, with a maximum amplitude ratio of 1.17D and an energy conversion percentage of up to 26.5%. Chizfahm et al. [21] studied the dynamic modeling of four configurations of the vortex-induced vibrations of a bladeless wind turbine and investigated the effects of the wind speed on the induced lift force, turbine deflection, and output power of four mast samples. The results of their studies showed that the performance of the rig with the conical geometry showed a higher performance than the rigs with the conventional circular cylinder [21]. The last example of the studies carried out on the geometry of objects in the range of high flow velocities (Reynolds number from 2000 to 50000) can be mentioned from the research of Zeng et al. [22], where the influence of the elastic modulus and mass ratio of the subject are studied. Also, they carried out numerical research on the two-dimensional simulation of cylindrical bodies with various cross-sections (circular cylinder, square, and circular prism). The Cir-Square cross section has the worst VIV effectiveness of the three cross-sectional geometries evaluated, with less than 0.2D in the amplitude response because of the place of its downward vortex shedding. But the Cir-Square cross section has the highest effectiveness compared to others.They came to the conclusion that a key component in developing the VIV response is the location of the vortex shedding brought on by the various cross-sectional forms [22].

According to the literature review, it seems that there is still a need to investigate the effect of the geometry of the objects exposed to the passage of the fluid flow and their influence on the resulting eddy currents behind the object. For this reason, in this research, two types of geometry: horizontal ellipse (H-ellipse) and vertical ellipse (V-ellipse) and their effects on displacement amplitude are investigated through the 2D simulation. The aim is to achieve the proper geometry in order to create favorable oscillation conditions in the body. For the purpose of generating a VIV response and extracting energy more successfully, a numerical research study is carried out to investigate the non-dimensional displacement amplitude and lift coefficient of flow past bluff objects.

2. Computational model and method

2.1. Cylinder motion

When a bluff body is placed in front of the fluid flow, the cylinder begins to oscillate due to the phenomenon of vortex shedding, because these vortices exert a periodic force on the surface of the bluff body [23]. This vortex-induced vibration phenomenon for a bluff body such as a cylinder depends on many parameters including drag and lift forces, stiffness, damping coefficient and mass ratio. There are various processes to investigate vortex-induced vibrations through simulating the motion of single or multiple degrees of freedom with numerical and experimental methods [24]. In this research the cylindrical structure is free only in the transverse direction. Structures that have a circular cross-section are used by many researchers to study vortex-induced vibrations for engineering applications. These systems can be modeled with a linear mass-spring system. In Fig. 1, the eddy vibration of a cylindrical section is shown as a 1DOF model for the movement in the transverse direction (**y**) as a mass-spring-damper system. Where $\boldsymbol{D}$ is the diameter of the cylinder, $\boldsymbol{k_s}$ is the stiffness coefficient and $\boldsymbol{c}$ is the damping coefficient [25]. These parameters were also used in the experimental studies of Hover *et al.* [26], Nguyen and Nguyen [27], and Bahadur Khan *et al.* [28].

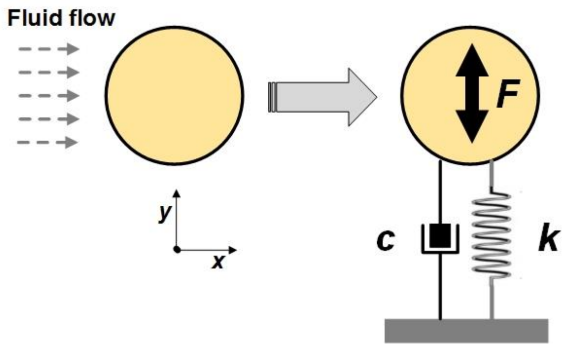

Figure 1. Schematics of the physical model [27].

Table 1 summarizes the main dimensionless parameters in the simulation of vortex-induced vibration systems used in this study, namely the Reynolds number ($\boldsymbol{Re}$), reduced velocity ($\boldsymbol{U_r}$), mass ratio ($\boldsymbol{m^*}$), which is the ratio of system's mass (cylinder mass) over the displaced fluid mass and dimensionless amplitude ratio $\boldsymbol{A}^*$ as given. $\boldsymbol{A}$ is the maximum range of displacement determined from the initial conditions of the system. The frequency ratio ($\boldsymbol{f^*}$) can also be seen in Table 1. The $\boldsymbol{f^*}$ is a dimensionless frequency that is defined based on the oscillation frequency of the body ($\boldsymbol{f}$) and the natural frequency of the system ($\boldsymbol{f_n}$). Also the drag ($\boldsymbol{C_D}$) and lift coefficients ($\boldsymbol{C_L}$) are presented in Table 1 [29].

Table 1. Number of the significant dimensionless parameters in the VIV flow.

Reynolds number	***Re***	$\mathrm{Re} = \frac{\mu UD}{\rho}$
Strouhal number	***St***	$St = \frac{fD}{U}$
Lift coefficient	$\boldsymbol{C_L}$	$C_L = \frac{F_L}{\frac{1}{2}\rho LDU^2}$
Drag coefficient	$\boldsymbol{C_D}$	$C_D = \frac{F_D}{\frac{1}{2}\rho LDU^2}$
Oscillation amplitude	$\boldsymbol{A^*}$	$A^* = \frac{A}{D}$
Mass ratio	m^*	$m^* = \frac{m}{\frac{1}{4}\pi\rho D^2 L}$
Frequency ratio	$\boldsymbol{f^*}$	$f^* = \frac{f}{f_n}$
Reduce velocity	$\boldsymbol{U_r}$	$U_r = \frac{U}{f_n D}$
Natural frequency	$\boldsymbol{f_n}$	$f_n = \frac{1}{2\pi}\sqrt{\frac{k}{m+m_A}}$

For the transient 2D viscous flow, the continuity and momentum equations are solved using ANSYS-FLUENT by employing the unsteady Reynolds-averaged Navier-Stokes (URANS) equations, the continuity and momentum equations were modified to calculate the turbulence in flow.

2.2. Description of the computational domain

In the present study, a rectangular computational domain was used . The 2D computational domain is represented in Fig .2. The size of the domain and the position of the cylinder have been chosen according to the simulations performed by Chizfahm et al. [21]. The computational domain with a width of W=120D and a stream-wise length of L=240D were designed, where D is the diameter of the body. The left and right sides of the computational domain are defined as velocity inlet and pressure outlet respectively. Upper and lower walls are defined as wall.

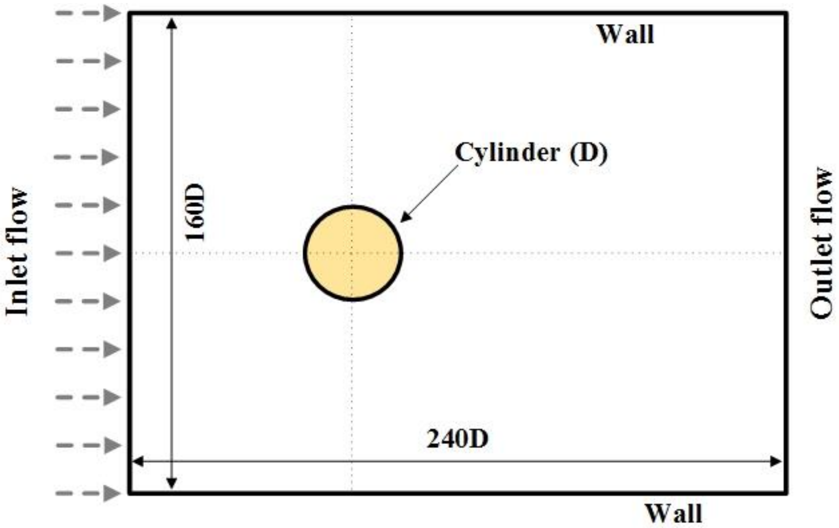

Figure 2. Domain of the computation and boundary conditions for the VIV of the bluff body.

Fig. 3 shows the three types of cross-sections for VIV bluff objects which included circle, H-ellipsoid and V-ellipsoid types. D represents the y-direction diameter of the bluff bodies. The diameter of these bluff objects is taken as D=0.18 m. In the numerical simulation, the inlet velocity is set to a uniform flow along the channel direction, and the velocity loss near wall caused by the viscosity of the fluid is also ignored .In this study a commercial CFD software ANSYS Fluent is used for all simulations.

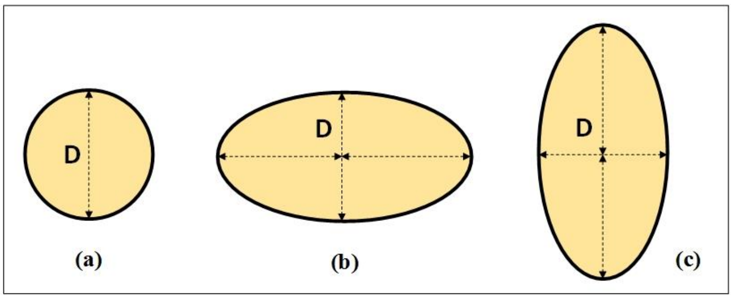

Figure 3. Bluff bodies: (a) Circle, (b) H-ellipsoid and (c) V-ellipsoid.

The simulations were done at about Re=51000. For an unsteady 2D viscous flow over a bluff body, the (URANS) equations can describe the flow properties. Also, the fluid flow is numerically simulated by using 2D URANS equations accompanied the k-ω Shear stress transport (SST) turbulence model [20]. In this study all simulations are performed with the SIMPLE pressure-velocity coupling algorithm. The spatial discretization scheme is chosen as the second-order upwind to maintain the accuracy and computational efficiency. The time step is different for each object and is chosen to keep the Courant number around 1. All the information related to the simulation setup according to the study by Chizfahmet al. [21] is given in Table 2.

Table 2. Physical model parameters for the simulation.

Simulation	2D
Reynolds number	51000
Domain	240D * 120D (D=0.18 m)
Number of elements	74776
UDF	Mass=0.1 kg f_n=2.0 Hz
Model	Viscous (*Kω -SST*)
Material (air)	ρ=1.2 kg / m^3 , 1.8 E-5 kg/m.s)
Boundary conditions	Inlet velocity (U_o)= 4.3 m/s
Dynamic mesh method	Smoothing /diffusion
Methods	Pressure-velocity coupling/Simple
Residuals	10^{-4}
Time step size	0.0008 s

It was considered that the free flow velocity and the velocity at the inlet border were equal. At the outflow boundary, the fluid velocity gradients in the stream direction were also found to be zero, and a reference value of zero was assigned to the pressure.

2.3. Computational mesh

Fig. 4 shows the quadrilateral structured mesh and also the close-up of the grid for different cross sections. Meshing was done with a quality of 90%. In the numerical simulation, the inlet velocity is set to a uniform flow along the channel direction, and the velocity loss near wall caused by the viscosity of the fluid is also ignored. Since a structured mesh was used in this work, the Smoothing method with the diffusion factor was chosen as a suggestion, because the mesh provides a more uniform deformation. To maintain the stability of the boundary layer, the diffusion parameter was set to 0.5. This numerical value of the diffusion parameter produces a more uniform deformation throughout the mesh. By setting the diffusion parameter to 0.5, the mesh becomes less deformed around the cylinder. Also, there is no structural damping in the motion of the cylinder and the damping is provided only by the viscosity of the fluid.

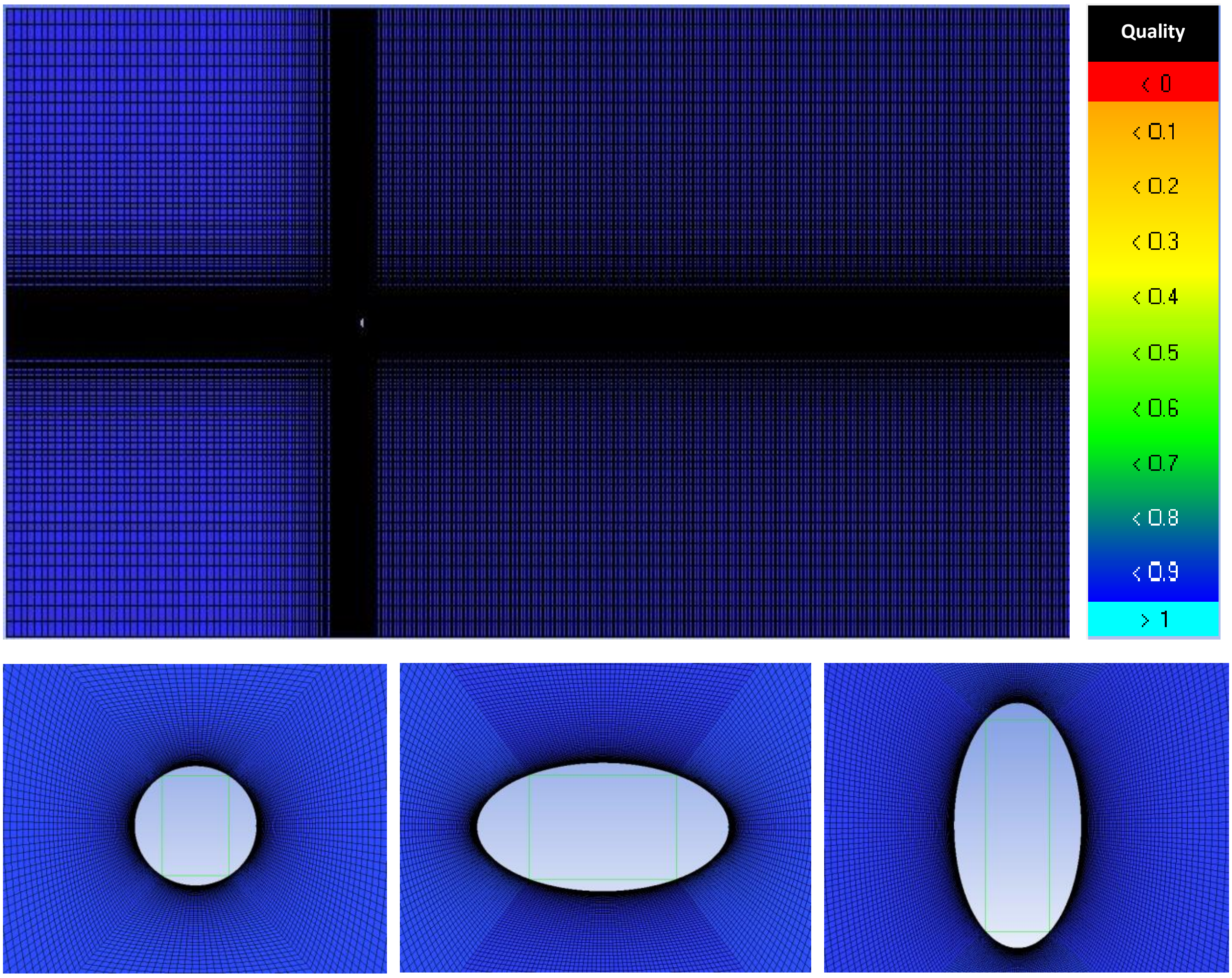

Figure 4. Close-up of the grid for different cross sections.

For studying the mesh independence, the relationship of the lift coefficient (C_L) and drag coefficient (C_D) response, with the grid number is investigated. A suitable mesh is obtained by repeating the computation to find a satisfactory independent grid. In order to simultaneously ensure the accuracy of the calculations and save the resources and calculation time as much as possible, the grid number of 80000 can be a good compromise between the precision and calculation time and is sufficient for carrying out the numerical simulation in the present work. For the cell counts greater than that, the grid size does not affect the results (the difference is less than 1%). So, the total number of cells in the whole model used in here is 80000 cells (Table 3).

Table 3. Mesh independence in the simulation.

Grid number	C_L	C_D
13000	0.2	2.53
30000	0.35	2.6
51000	0.47	2.72
80000	0.6	2.74
100000	0.62	2.76
120000	0.63	2.76
130000	0.61	2.755

2.4. Model validation

The study by Asyikin [30] has been selected for validation. All of the simulation characteristics, such as the diameter of the cylinder ***D***, density, natural frequency of the structure and Reynolds number, match the Asyikin model exactly [30]. The simulations are in the Reynolds numbers of 1000 to 200, and the U=1 m/s was taken into account for the corresponding velocity in the x-direction. Also, a rectangular domain with the dimensions of 60D by 90D was used for the simulation. The numerical results of the displacement amplitude, and C_L of this study have been compared with the same in the study by Asyikin [30], and showed a good agreement.

3. Results and discussion

3.1. Oscillation response for the VIV of the circular cylinder

In this research, the two-dimensional VIV simulation of the bladeless wind turbine oscillation was performed at the Reynolds number of 51000, using the ANSYS FLUENT software. Also there is no structural damping in the movement of the cylinder. Fig. 5 shows the velocity contours and the development of the displacement of the cylinder in the direction of the cross flow as a function of the flow time. It can be seen from the same that the vortices behind the cylinder were completely formed in 5 s, and the object was oscillating. The reaction of the cylinder increases at a few seconds after the force being exerted. The reason for this phenomenon is that when the fluid flow passes over the cylinder, vortices are created and the vortex shedding and lift force cause the object to oscillate.

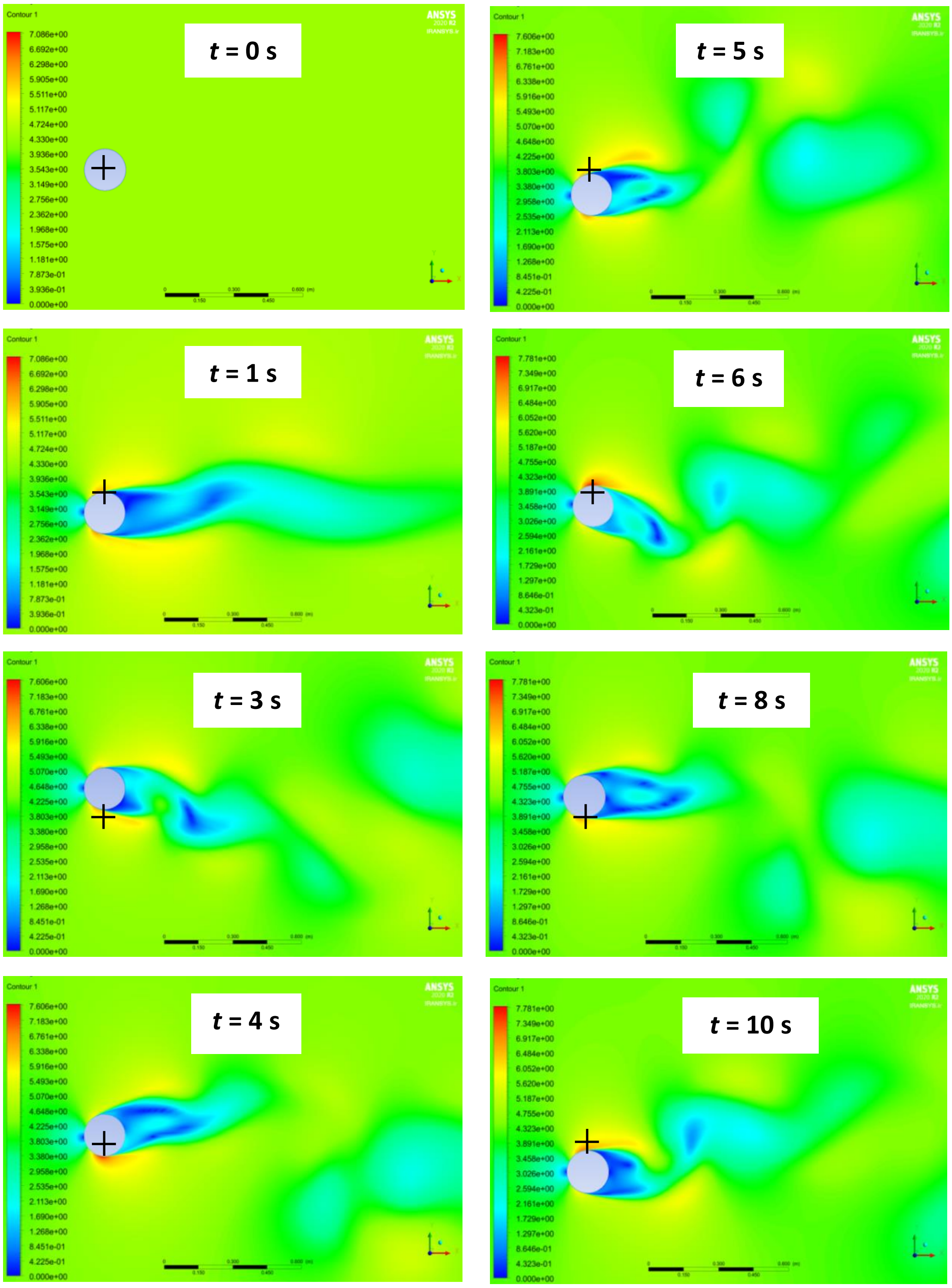

Figure 5. (a) Amplitude ratio and (b) lift coefficients for the VIV acting on the circular cylinder versus the flow time.

Fig. 6 shows the results of the displacement value (A/D) and C_L coefficient , according to the time and under the oscillatory conditions. It is clear that the magnitude of the displacement is in the range of 0.1 to -0.1. Also, the value of the $\boldsymbol{C_L}$ coefficient is in the range of 1.5 to -1.5.

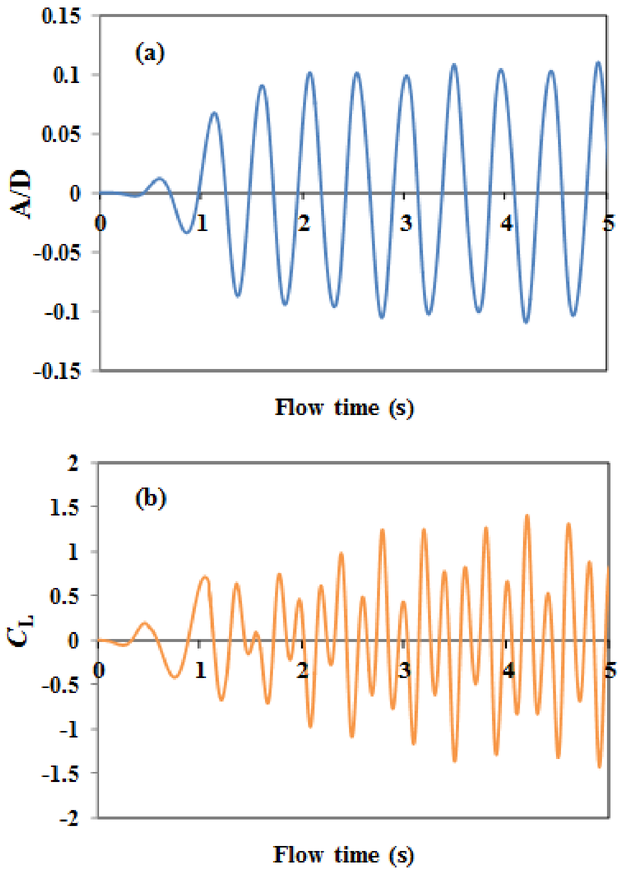

Figure 6. Wake 2D patterns for the VIV of the circle at the Re=51000 and different flow times.

3.2. Oscillation response for the VIV of different geometries

In this section, the VIV simulation of three types of cross-section objects including circle, H-ellipsoid, and V-ellipsoid have been done. The features of the flow pattern, the amount of the displacement of the body, as well as the coefficients of the applied lift force have been investigated. The results related to the formation of vortices at the beginning of the flow in different geometries with bluff cross sections, and their comparison are shown. Fig. 7 shows the variation of the displacement amplitude and lift coefficient for three types of geometry under the conditions of the Reynols number of 51000 As seen in Fig. 7, the time required for each case to initiate the displacement of the bluff bodies is different from that of others. These initiations are strongly associated with the frequency of the vibration. Also, the vortex shedding for each case that forms behind these bluff bodies is different from the same for others, and the surface of the bluff bodies, through which the fluid passes, for each case is also different from that for other cases. These differences show that the ranges of their movements are also different. It can be said that the type of the geometry plays a very important role in the displacement amplitude of the object.

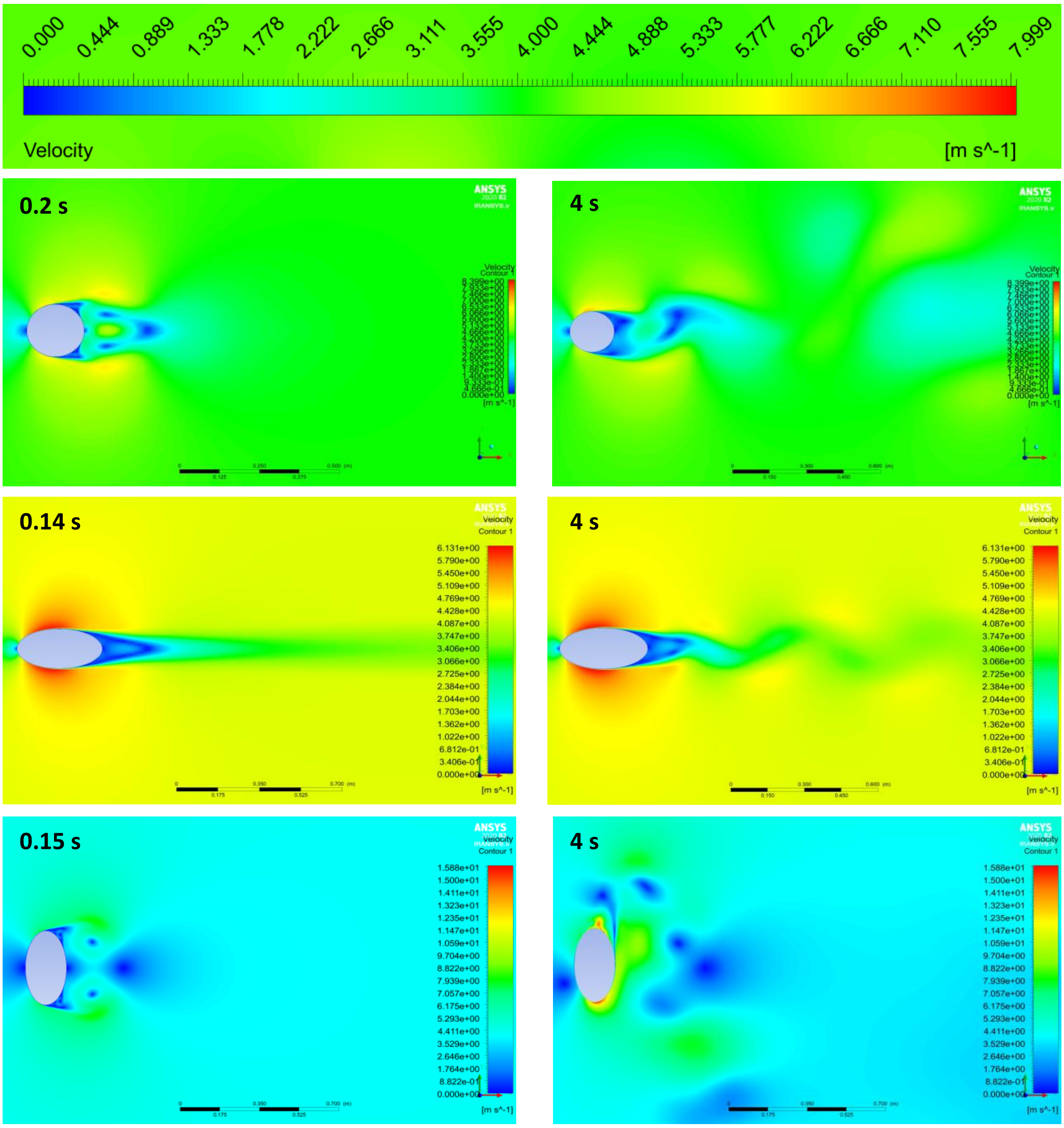

Figure 7. Wake patterns for the VIV with different geometries at the initiation of the procedure and t=4 s of the flow time (Re=51000)..

Fig. 8 shows the variation of the displacement amplitude and lift coefficient for three types of geometry under the conditions of the Reynols number of 51000. As it can be seen in Fig. 8, the length of the displacement and the lift coefficient in the H-ellipsoid shape have the lowest values and the displacement fluctuations have also the lowest numbers. Also the geometry of the V-ellipsoid shape has the highest values of the displacement amplitude and lift coefficient. It is because of the type of geometry. The V-ellipsoid shape has bigger surface area. When the fluid passes through the bluff cross section, there is stronger vortex shedding created, and due to the pressure difference and lift force created, it oscillates the object in a higher range of displacements.

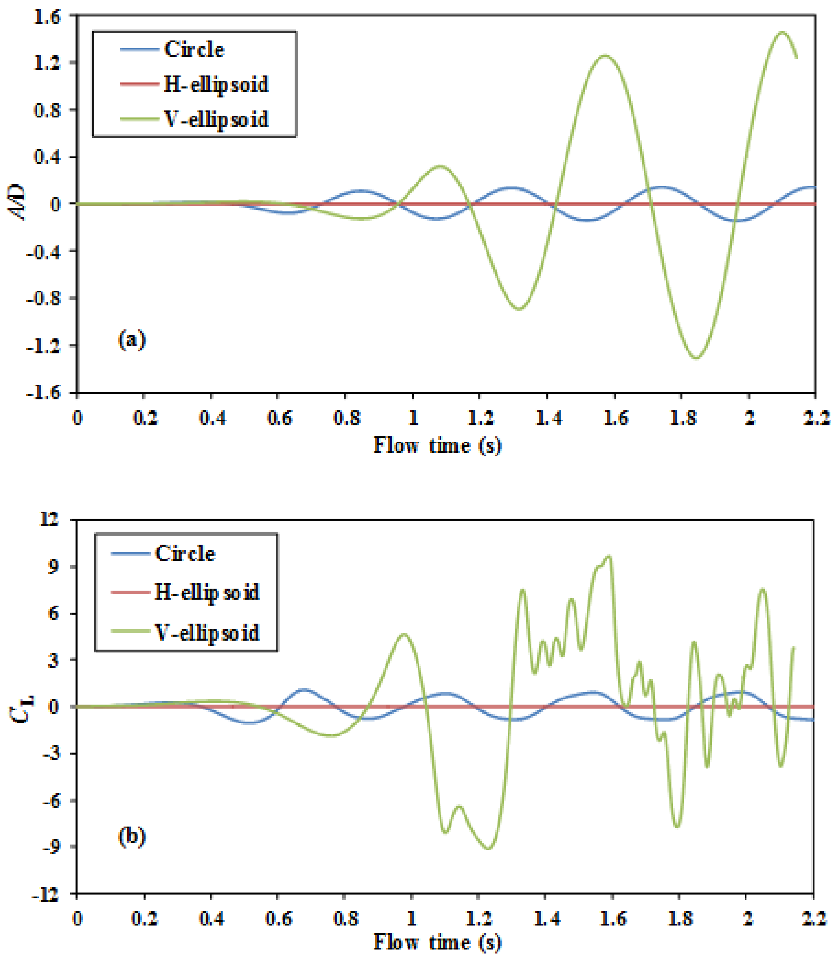

Figure 8. (a) Amplitude ratio and (b) lift coefficients for the VIV with different geometries at the initiation of the procedure and t=2.2 s of flow time (Re=51000).

3.3. Oscillation response for the VIV of a V-ellipsoid geometry

Due to the fact that the V-ellipsoid geometry showed the maximum range of displacement compared to other geometries, , the effect of the most important dimensionless parameter, i.e the Reynolds number on this geometry, is examined. The viscosity patterns of vortices for the V-ellipsoid geometry in different reynolds numbers are shown in Fig. 9. For each reynolds number, the pattern of vortices is different from that of others. Additionally, the contours of vortices reveal that they are dispersed behind the body in the area known as the Karman vortex street. The rapid diffusion could be brought on by the artificial diffusion setting of simulations. Whether a higher-order discretization technique or an increase in the mesh density, in the region behind the bluff body can be used to solve this problem .

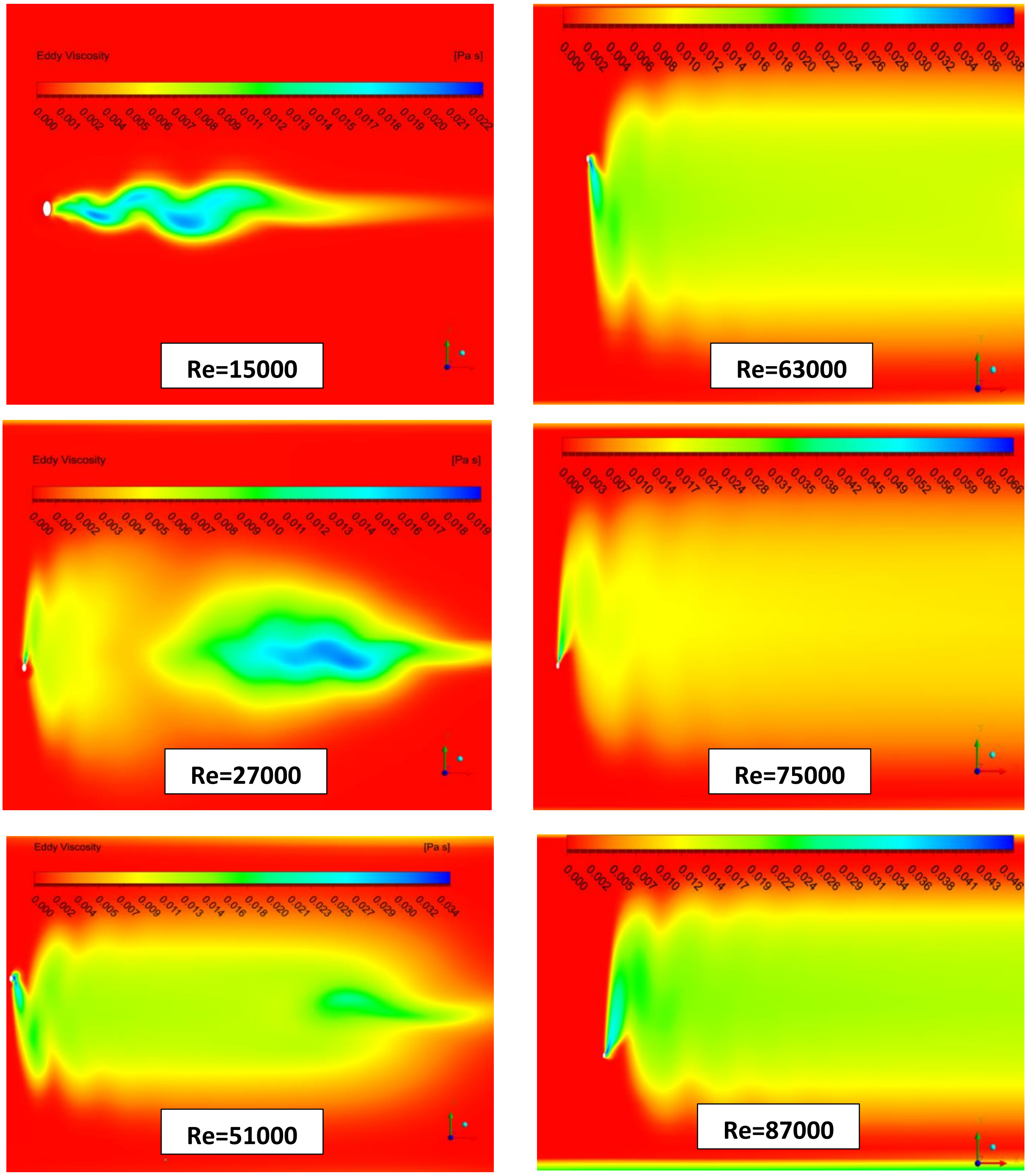

Figure 9. Eddy viscosity and wake pattern for the VIV of the V-ellipsoid shape at different Reynolds numbers.

The variation of the amplitude of the displacement and the lift coefficient in order to assess the performance of the vertical elliptical shape in various Reynolds numbers are presented in Fig. 10. According to the results related to the variations of the displacement range with respect to different Reynolds numbers as shown in Figure 10, for the mentioned geometry, the value of the displacement range as well as the numerical value of the lift coefficient have increased. Though it has a stronger reaction of the displacement amplitude in the higher Reynolds numbers, it is important to remember that the system's operating conditions are constrained, and the equipment needs to be able to endure the wind blowing at such high speeds.

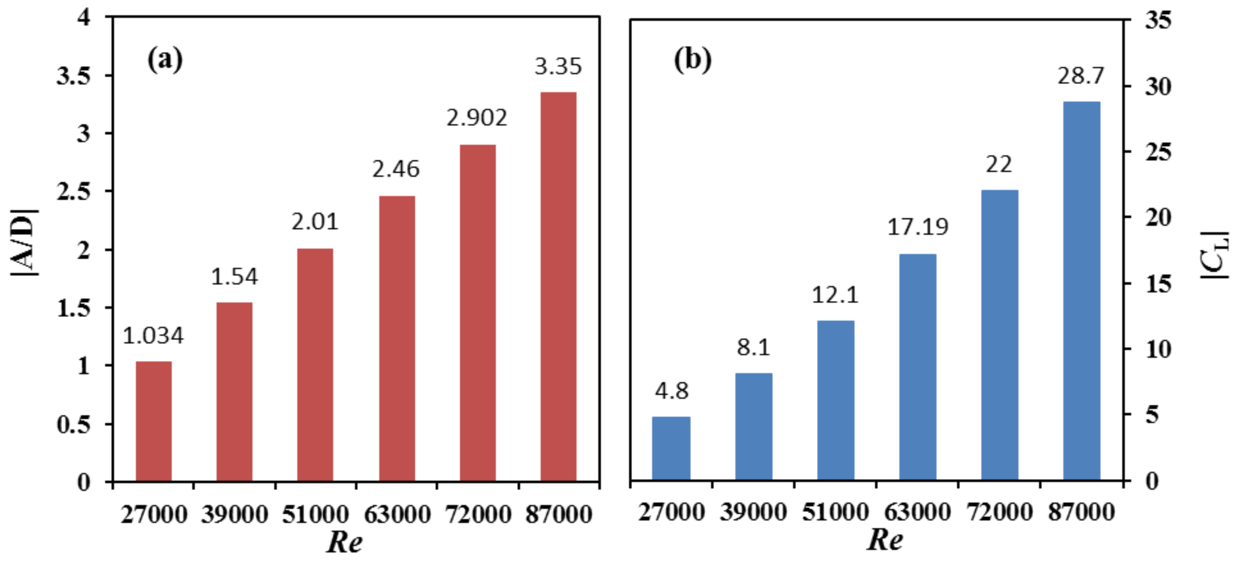

Figure 10. Amplitude ratio and (b) C_L for the VIV of V-ellipsoid geometry vs. the Reynolds number.

4. Conclusion

The two-dimensional simulation of the bladeless wind turbine oscillation at the Reynolds number of 51600 was carried out. First, the vortex-induced vibration simulation for the cylinder was done. The vortices contures at the start of the oscillation in 0.2 seconds and the formation of the full vortex flow and system oscillation were visible in the fifth second. It was also observed that the changes in the values of displacement and lift coefficient are 0.1 and 1-1.5 respectively. Next, the CFD simulation of the bladeless wind turbine oscillation in the geometries of circle, H-ellipsoid, and V-ellipsoid was investigated, and the results related to the velocity contours, variation in displacement amplitude, and lift coefficient value for each geometry were studied. According to the results, it was observed that the V-ellipsoid shape had higher values of the displacement amplitude and lift coefficient than other geometries. Therefore, this geometry was chosen to investigate the effect of the Reynolds number parameter in the wide range of 27000 to 87000. It was also determined that the displacement value and the lift coefficient's numerical value increased as the Reynolds number increased.

Acknowledgements

The authors are grateful to Razi university for the financial support they extended towards this project.

Nomenclature

A	Maximum amplitude
A^*	Amplitude ratio
c	Damping coefficient
C_L	Lift coefficients
C_D	Drag coefficients
D	Cylinder's diameter
f	Frequency of the body oscillates
F	Fluid forces
F_o	Maximum force
F_D	Drag force
F_L	Lift force
f_n	Natural frequency
f^*	Frequency ratio
g	Gravitational acceleration
k	Stiffness coefficient
L	Cylinder's length

m	Cylinder's mass
m_A	Cylinder's added mass
m_d	Displaced fluid mass
m^*	Mass ratio of the flexible bluff
p	Pressure
Re	Reynolds number
St	Strouhal number
t	Time
U	Uniform inlet fluid velocity
Ur	Reduced velocity
y	Cylinder motion direction
ρ	Fluid density
μ	Fluid viscosity
v	Kinematic viscosity

References

[1] Aizpurua J.L., Peña-Alzola R., Olano J., Ramirez I., Laza I., Rio L.D. and Dragicevic T., "Probabilistic machine learning aided transformer lifetime prediction framework for wind energy systems", Int. J. Electr. Power Energy Syst., 153, 10935 (2023).

[2] Ellabban O., Abu-Rub H. and Blaabjerg F., "Renewable energy resources: Current status, future prospects and their enabling technology", Renew. Sustain. Energy Rev., 39, 748 (2014).

[3] Liu R., Peng L., Huang G., Zhou X., Yang Q. and Cai J., "A Monte Carlo simulation method for probabilistic evaluation of annual energy production of wind farm considering wind flow model and wake effect", Energy Convers. Manag., 292, 117355 (2023).

[4] Aghaei V.T., Ağababaoğlu A., Bawo B., Naseradinmousavi P., Yıldırım S., Yeşilyurt S. and Onat A., "Energy optimization of wind turbines via a neural control policy based on reinforcement learning Markov chain Monte Carlo algorithm", Appl. Energy, 341, 121108 (2023).

[5] Al-Obaidi M.A., Alsarayreh A.A., Bdour A., Jassam S.H., Rashid F.L. and Mujtaba I.M., "Simulation and optimisation of a medium scale reverse osmosis brackish water desalination system under variable feed quality: Energy saving and maintenance opportunity", Desalination, 565, 116831 (2023).

[6] Viré A., Derksen A., Folkersma M. and Sarwar K., "Two-dimensional numerical simulations of vortex-induced vibrations for a cylinder in conditions representative of wind turbine towers", Wind Energy Sci., 5, 793 (2020).

[7] Beran V., Sedlácek M. and Marsik F., "A new bladeless hydraulic turbine", Appl. Energy, 104, 978 (2013).

[8] Francis S., Umesh V. and Shivakumar S., "Design and analysis of vortex bladeless wind turbine", Mater. Today: Proceed., 47, 5584 (2021).

[9] Song Y., Du M., Zhao W. and Lin H., "A new integrated regulation strategy and modelling for wind turbine with battery energy storage system", J. Energy Storag., 63, 107111 (2023).

[10] Yang J. and Lin T., "Novel calculation method for windage power loss of double-helical gear transmission", J. Fluid. Eng., 145(12), 121201 (2023).

[11] Braun J., Falempin F. and Paniagua G., "Energy analysis of a detonation combustor with a bladeless turbine, a propulsion unit for subsonic to hypersonic flight", Energy Convers. Manag., 262, 115491 (2022).

[12] Seyed-Aghazadeh B., Carlson D.W. and Modarres-Sadeghi Y., "The influence of taper ratio on vortex-induced vibration of tapered cylinders in the crossflow direction", J. Fluid. Struct., 53, 84 (2015).

[13] Zhao D., Ji C., Teo C. and Li S., "Performance of small-scale bladeless electromagnetic energy harvesters driven by water or air", Energy, 74, pp. 99 (2014).

[14] Blevins R.D., "Models for vortex-induced vibration of cylinders based on measured

forces", J. Fluid. Eng., 131(10), 101203 (2009).

[15] Misaka T., "Estimation of vortex-induced vibration based on observed wakes using computational fluid dynamics-trained deep neural network", J. Fluid. Eng., 143(10), 104501 (2021).

[16] Rashki M.R., Hejazi K., Tamimi V., Zeinoddini M. and Aalami Harandi M.M., "Impacts of soft marine fouling on the hydrokinetic energy harvesting from one-degree-of-freedom vortex-induced vibrations", Sustain. Energy Technol. Assess., 54, 102881 (2022).

[17] Modir A., Kahrom M. and Farshidianfar A., "Mass ratio effect on vortex induced vibration of a flexibly mounted circular cylinder, an experimental study", Int. J. Mar. Energy, 16, 1 (2016).

[18] Gohate G., Bobde S., Khairkar A. and Jadhav S., "Study of vortex induced vibrations for harvesting energy", Int. J. Innov. Res. Sci. Technol., 2(11), 374 (2016).

[19] Zhang B.S., Song B.W., Mao Z.Y., Tian W.L. and Li B.Y., "Numerical investigation on VIV energy harvesting of bluff bodies with different cross sections in tandem arrangement", Energy, 133(15), 723 (2017).

[20] Zhang B.S., Mao Z.Y., Song B.W., Tian W.L. and Ding W.J., "Numerical investigation on VIV energy harvesting of four cylinders in close staggered formation", Ocean Eng., 165, 55 (2018).

[21] Chizfahm A., Azadi Yazdi E. and Eghtesad M., "Dynamic modeling of vortex induced vibration wind turbines", Renew. Energy, 121, 632 (2018).

[22] Zheng M., Han D., Gao S. and Wang J., "Numerical investigation of bluff body for vortex induced vibration energy harvesting", Ocean Eng., 213, 107624 (2020).

[23] Govardhan R. and Williamson C.H.K., "Modes of vortex formation and frequency response of a freely vibrating cylinder", J. Fluid. Mech., 420, 85 (2000).

[24] Khalak A., Williamson C.H.K., "Dynamics of a hydroelastic cylinder with very low mass and damping", J. Fluid. Struct., 10(5), 455 (1996).

[25] Sarpkaya T., "A critical review of the intrinsic nature of vortex-induced vibrations", J. Fluid. Struct., 19 (4), 389 (2004).

[26] Hover F., Miller S. and Triantafyllou M., "Vortex-induced vibration of marine cables: experiments using force feedback", J. Fluid. struct., 11(3) 307 (1997).

[27] Nguyen V.T. and Nguyen H.H., "Detached eddy simulations of flow induced vibrations of circular cylinders at high Reynolds numbers", J. Fluids Struct., 63, 103 (2016).

[28] Bahadur Khan N., Ibrahim Z., The Nguyen L.T., Javed M.F. and Ali J., "Numerical investigation of the vortex-induced vibration of an elastically mounted circular cylinder at high Reynolds number (Re = 104) and low mass ratio using the RANS code", PLOS ONE, 12(10) e0185832 (2017).

[29] Mutlu A.O., Bayraktar M. and Bayraktar S., "Two-dimensional simulations of vortex-induced vibration of a circular cylinder", Proceed. Ins. Mechan. Eng., Part M: J. Eng Marit. Environ., 235(3), 683 (2021).

[30] Asyikin M.T., "CFD Simulation of Vortex Induced Vibration of a Cylindrical Structure," MS thesis, Dep. Civil Trans. Eng., Norwegian University of Science and Technology (2012).